AD-A182 389 FREE-WAKE ANALYSIS OF A ROTOR IN HOVER(U) OHIO STATE UNIV COLUMBUS C S CHEN ET AL. 1987 1/1

UNCLASSIFIED F/G 20/4 NL

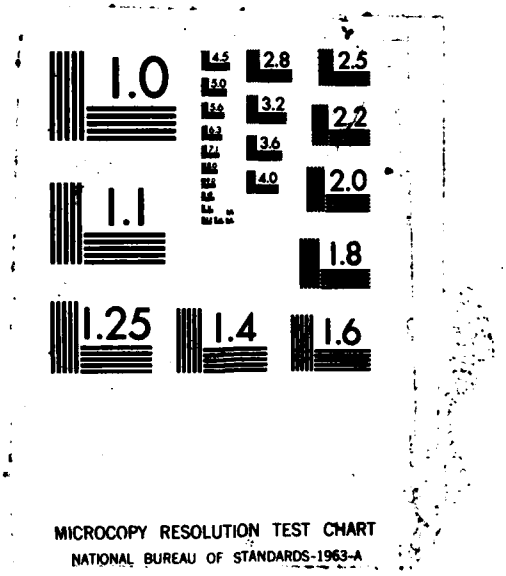

AIAA'87

AIAA-87-1245

FREE-WAKE ANALYSIS OF A ROTOR IN HOVER

C. S. Chen
Ohio State University
Columbus, Ohio

H. R. Velkoff
Ohio State University
Columbus, Ohio

C. Tung
Aeroflightdynamics Directorate
U.S. Army Aviation Research and Technology Activity
Ames Research Center
Moffett Field, California

AIAA 19th Fluid Dynamics, Plasma Dynamics and Lasers Conference
June 8-10, 1987/Honolulu, Hawaii

FREE-WAKE ANALYSIS OF A ROTOR IN HOVER

C.S. Chen† and H.R. Velkoff‡
The Ohio State University
Columbus, Ohio

and

C. Tung*
Aeroflightdynamics Directorate
U.S. Army Aviation Research and Technology Activity
Ames Research Center
Moffett Field, California

Abstract

A numerical method based on the axisymmetric, incompressible Navier-Stokes equations is combined with a lifting surface code to predict the vortex wake of hovering rotors. The lifting surface code, AMI Hover, is used to obtain the circulation distribution on the blade. This circulation distribution is fed into the Navier-Stokes code to compute the vortex wake under this specified circulation distribution. An iteration approach is used between these two codes to converge the circulation distribution and the shape of the vortex wake. A relaxation scheme is developed to resolve the instability encountered among the tip vortices. A reconcentration scheme is used to solve the diffusion problem due to the strong artificial viscosity. The results from the present method are compared with experimental data obtained by smoke-flow visualization and hot-wire measurements for several rotor blade configurations. The comparisons show that the present method is able to predict the complex wake system shed by a hovering rotor.

Introduction

Vortex-dominated flow fields are frequently encountered in the flight operations of fixed- or rotary-wing aircraft. The vortex wake shed by a hovering rotor is one of the most complex flow fields in aerodynamics because of the highly nonlinear interaction within the wake system and with the rotor. Complete prediction of the flow field is difficult, since the wake system is extremely unstable as is confirmed by experiment. The difficulty also lies in the uncertainties encountered in predicting the flow field, such as the appropriate model of the far wake and the disparate length scales associated with the generation, interaction, and eventual decay of the vortices.

However, hover capability is one of the most important design goals for helicopters and other vertical take off and landing (VTOL) aircraft, since these aircraft are designed to take off and land vertically, and to hover for a relatively long time for rescue attempts and other purposes. Hover performance prediction is also essential because of the payload to gross-weight ratio of such aircraft and the requirement to hover out of ground effect. In predicting the performance of helicopters, the vortex wake shed by the blades is a crucial element because it stays close to the rotor plane and has a strong interaction with the blades. In fact, the vortex wake is an important element in all helicopter problems including performance, structural loads, vibration, stability, and noise.

Methods which assume the vortex interactions to be inviscid have proven very useful. The flow field is represented as a series of point or line vortices, then traced in a Lagrangian frame. Unfortunately, a substantial amount of numerical damping is required to converge the solution because of the singular behavior of the point or line vortex; this numerical damping might disturb the force-free conditions of the flow field. Panel methods have been successful in predicting the performance of a hovering rotor, but their role in free-wake prediction is less satisfactory.

The present method represents the vortex wake as a continuous distribution of vorticity. A Gaussian distribution of vorticity is assumed across the vortex wake. The vorticities are traced in an Eulerian frame. The movement of the vortex wake is governed by the incompressible, axisymmetric Navier-Stokes equations. It was found that representing the vortex wake as a continuous distribution of vorticity is more successful than representing it as a series of point or line vortices. The reason is that representing a vortex sheet as a layer of continuous distributing vorticity eliminates singularities in the computational domain. Although there is still instability among the tip vortices, there is no instability in the inboard vortex sheets. Some of the tip vortex instabilities observed in numerical simulations closely resemble those observed in hover tests. The numerical tip-vortex instability may be caused by the unstable characteristics of the wake system, and not necessarily by the numerical scheme. A relaxation scheme is used in the iteration procedure to stabilize the tip vortices. Diffusion or artificial viscosity was another problem encountered in this work, which was solved by periodically applying a reconcentration scheme.

Governing Equations

The assumptions and governing equations are described below. In the calculation of the vortex wake shed by a fixed-wing aircraft, it is often assumed that the streamwise gradients are small. In the case of a rotor in hover, an analogous assumption is made; that because the circumferential gradients are small, the streamwise development of the vortex wake can be reduced to a time-dependent axisymmetric calculation [1].

The flow is assumed to be viscous and incompressible. If the flow field is observed from an inertial cylindrical coordinate system ((r, θ, z) where r and θ define the plane of the rotor rotating about the vertical axis z), the flow field induced by a rotor in hover is unsteady and three-dimensional. If observed from a noninertial coordinate system rotating with the rotor blade, the flow field appears to be steady and three-dimensional. The inertial coordinate system is converted into

---

† Research Associate, Mechanical Engineering Department.

‡ Professor, Mechanical Engineering Department.

* Research Scientist. Member AIAA.

a noninertial coordinate system by applying the following conditions

$$\begin{aligned} r &= r \\ \phi &= \theta - \Omega t \\ z &= z \\ t &= t \end{aligned}$$

The rotor blade rotates with angular speed Ω about the $z-$axis. The three-dimensional flow field is further reduced to an unsteady axisymmetric flow field by assuming (1) the circumferential velocity component and pressure gradient are negligible and (2) the rate of change of the velocity gradients in the circumferential direction is small

$$v = \frac{1}{r}\frac{\partial p}{\partial \phi} = \frac{1}{r^2}\frac{\partial^2 u}{\partial \phi^2} = \frac{1}{r^2}\frac{\partial^2 w}{\partial \phi^2} = 0 \qquad (1)$$

where u, v, and w are velocities in the r, θ, and z directions, and p is pressure. This assumption is a straightforward extension of a practice commonly used in fixed-wing analysis to reduce the steady three-dimensional vortex wake roll-up calculation to an unsteady two-dimensional calculation. The development over time of the two-dimensional (in the case of fixed-wing) or axisymmetric (in the case of a rotor in hover) flow field represents the streamwise development of the three-dimensional flow. The resulting axisymmetric continuity and momentum equations are given below

$$\frac{1}{r}\frac{\partial (ru)}{\partial r} + \frac{\partial w}{\partial z} = 0 \qquad (2)$$

$$\Omega\frac{\partial u}{\partial \phi} - u\frac{\partial u}{\partial r} - w\frac{\partial u}{\partial z} = \frac{1}{\rho}\frac{\partial p}{\partial r} - \nu\left(\nabla^2 u - \frac{u}{r^2}\right) \qquad (3)$$

$$\frac{1}{\rho r}\frac{\partial p}{\partial \phi} = 0 \qquad (4)$$

$$\Omega\frac{\partial w}{\partial \phi} - u\frac{\partial w}{\partial r} - w\frac{\partial w}{\partial z} = \frac{1}{\rho}\frac{\partial p}{\partial z} - \nu\nabla^2 w \qquad (5)$$

and the axisymmetric Laplacian operator is

$$\nabla^2 = \frac{1}{r}\frac{\partial}{\partial r}\left(r\frac{\partial}{\partial r}\right) + \frac{\partial^2}{\partial z^2} \qquad (6)$$

Note that the above equations are time-like in the variable ϕ representing circumferential development of the flow. Equations (2)-(5) can be efficiently solved in vorticity-stream-function form as below

$$\Omega\frac{\partial \zeta}{\partial \phi} - \frac{\partial (u\zeta)}{\partial r} - \frac{\partial (w\zeta)}{\partial z} = -\nu\left(\nabla^2\zeta - \frac{\zeta}{r^2}\right) \qquad (7)$$

$$\nabla^2\psi - \frac{2}{r}\frac{\partial \psi}{\partial r} = -\zeta r \qquad (8)$$

where ψ is the stream function, and the vorticity is defined as

$$\zeta = \frac{\partial u}{\partial z} - \frac{\partial w}{\partial r} \qquad (9)$$

the velocities are defined as

$$u = -\frac{1}{r}\frac{\partial \psi}{\partial z} \qquad (10)$$

$$w = \frac{1}{r}\frac{\partial \psi}{\partial r} \qquad (11)$$

The assumption that $v = 0$ essentially limits the analysis to locations outside the boundary layer of the blades. Equations (7) and (8) together with the initial and boundary conditions constitute an initial-boundary-value problem. The initial condition corresponds physically to the vorticity distribution at $\phi = 0$ and a small distance circumferentially downstream of the rotor-blade trailing edge. The initial vorticity distribution must be obtained by other means, such as from experimental data or numerical lifting-surface (or lifting-line) calculation. A lifting-surface calculation [2] of the blade load distribution is used to determine the initial vorticity distribution in the present work.

Two sets of boundary values are required in the calculations. One is the set of boundary values of vorticity for the vorticity transport equation. The other is the set of boundary values of stream function for the Poisson equation. The vortices shed by a blade are modeled by the Lamb vortex [3].

$$\zeta(r,t) = \frac{\Gamma}{4\pi\nu t}\exp\frac{-r_d^2}{4\nu t} \qquad (12)$$

$$r_c^2 = 4\nu t \qquad (13)$$

where r_d is the radius from the center of each vortex, r_c is the core radius which gives the location of the maximum velocity of the vortex, and ν is the kinematic or eddy viscosity. The circulation strength of the vortex is Γ, which is determined by the circulation difference of the neighboring points on the blade.

For each Lamb vortex, the vorticity decays exponentially from its center

$$\zeta = O(\exp(d^{-2})) \qquad \text{as} \qquad d = (r^2 + z^2)^{1/2} \longrightarrow \infty \qquad (14)$$

Therefore, zero vorticity is used on the boundary and is considered as a reasonable assumption as long as the boundary is sufficiently long.

For circular vortices in an unbounded domain in which fluid particles come to rest far away from the vortices, the stream function can be obtained by [4]

$$\begin{aligned} \psi(z,r,t) &= \frac{r}{4\pi}\int_{-\infty}^{\infty}\int_0^{\infty}\int_0^{2\pi}\frac{r'\zeta(z',r',t)\cos\theta}{\xi}\,dz'\,dr'\,d\theta \\ &= \frac{r}{4\pi}\int_{-\infty}^{\infty}dz'\int_0^{\infty}r'\,dr'\,\zeta(z',r',t)\int_0^{2\pi}\frac{\cos\theta}{\xi}\,d\theta \end{aligned} \qquad (15)$$

where

$$\xi = |(z-z')^2 + r^2 + r'^2 - 2rr'\cos\theta|^{1/2} \qquad (16)$$

and $\zeta(z',r',t)$ is the value of the vorticity at position (z',r') and time t.

The above equation can be expanded as a series solution if the boundary extends a sufficient distance [5]. A very efficient technique is to obtain the boundary values by a series solution. For the present problem, a small grid size is necessary to resolve the flow field since the extent of the boundary is not suitable for the series solution. Direct integration of Eq. (15) is used to obtain the boundary values of the stream function for small grid sizes.

Two finite-difference methods are combined to solve the vorticity transport equation. One is the DuFort-Frankel method and the other is the alternating-direction-implicit method. Although the DuFort-Frankel method is suitable for this problem, it requires the solution of the current and the last time steps to solve for the solution of the next time step. For the present problem, which is a periodic problem, only the information of the current flow field is known at each new cycle; the information of the flow field one time-step before is unclear. In the computation, a new layer of vorticity of the same strength and distribution as the initial vorticity is added to the computational domain to represent the vortex sheet shed by the passing blade. This new layer of vorticity is added at exactly the time when a blade passes by. At that moment, the only information known is that a vortex sheet has been shed by the

blade; there is no information one time-step ahead. Therefore, another method is needed to calculate the flow field at the begining of each new cycle. The alternating-direction-implicit method is chosen to accomplish this task, because this method requires only the solution of the present time-step to find the solution of the next time-step.

Computational Procedures

The computational procedures of the Navier-Stokes calculations are described in this section. The calculation starts by estimating the shape of the vortex wake. This shape is used as the input to the lifting surface code, AMI Hover, to obtain the circulation distribution on the blade. The circulation distribution is then used as the input to the Navier-Stokes calculation. The calculation is terminated when the shape of the vortex wake under this specified circulation distribution converges. The converged wake shape is again used as the input to the AMI Hover code. The output or the circulation distribution is then used as the input to the Navier-Stokes calculation. This process is repeated until both the shape of the vortex wake and the circulation distribution on the blade converge. If an uncontracted vortex wake is assumed as the initial wake, it usually takes seven iterations to converge the results for two-bladed rotors and nine iterations for four-bladed rotors. If a better initial condition, such as the wake described by Landgrebe's generalized wake equations [6], is used, it requires only three to four iterations.

An iteration approach is used inside the Navier-Stokes calculations. The calculation starts by distributing five to eight free-to-move vortex sheets. Each vortex sheet is represented by the superposition of a series of Lamb vortices. The strengths of the Lamb vortices are determined by the change in load distribution (obtained from the AMI Hover code) between grid points with the core radius of each vortex prescribed to be a fixed percentage (in this case, 2%) of the blade radius R. Initially, the geometry of these vortex sheets is described by Landgrebe's prescribed wake equations [6], but the shape of the wake is determined by the mutual interaction of the wake element after the calculation begins. A semi-infinite vortex cylinder is chosen as the far wake and is placed below these free-to-move vortex sheets with its radius equal to the radius of the tip vortex of the last free-vortex sheet and its unit strength determined by the strength and descending velocity of the last free-tip vortex. At the time corresponding to a blade passage, the last free-vortex sheet is removed and a new vortex sheet, the same as the initial vortex sheet that was placed on the rotor plane, is added to the rotor plane, keeping the number of the free-vortex sheets constant. The relaxation scheme (which will be explained later) is also applied to the tip vortices at this time to prevent the instability from growing. The vortex wake is force-free and moves by its own interaction between blade passages. It takes about 20 min of CPU time for the Cray X-MP/48 to converge a vortex wake by the Navier-Stokes calculations.

The vortex wake is integrated step by step between any two blade passages. At each time step, the computational procedure is:

1. Calculate the boundary values of the stream function by using Eq. (15).
2. Solve the Poisson equation, Eq. (8), to obtain the stream function.
3. Obtain the velocity field from the stream-function field.
4. Integrate the vortex wake one step forward by the vorticity transport equation (Eq. (7)). The time step is determined by the numerical stability criterion imposed by the Dufort-Frankel method.

This process is repeated until another blade passes by. Typically it takes about 50 time steps to integrate the vortex wake from one blade passage to another for a two-bladed rotor.

Relaxation and Reconcentration

The vortex wake of a hovering rotor is extremely unstable; a small perturbation can stimulate the instability, as is also confirmed by experiment. The instability of small perturbations to the vortex wake of a hovering rotor was investigated by Bliss et al. [7]. They converted the stability problem into an eigenvalue problem and solved it numerically. They found that most of the eigenvalues were complex and many had positive real parts, which indicates numerous unstable modes. Therefore a time-marching approach is probably not adequate for this problem, since this approach assumes the system is stable and the perturbations will be damped out during the marching process. But the vortex wake of a hovering rotor is unstable. Since the tip vortices are the source of the instability, an iteration approach plus a relaxation scheme are used to investigate this problem.

In the iteration approach, a new layer of vorticity (or a vortex sheet) identical to the one initially placed on the rotor plane is added to the rotor plane at the time corresponding to a blade passage. Then the last layer of vorticity (an inboard vortex sheet plus a tip vortex) is removed, keeping the number of vorticity layers constant. The corresponding initial-vorticity distribution is generated by summing a series of individual Lamb vortices along the computational grid representing the rotor blade [1]. Between blade passages, the flow field is force-free, i.e., the vortices move according to their mutual interactions. Whenever a blade passes by, the positions of the tip vortices are relaxed by the following formula

$$r_T^{new} = r_T^{old} + \omega(r_T^{present} - r_T^{old}) \tag{17}$$

$$z_T^{new} = z_T^{old} + \omega(z_T^{present} - z_T^{old}) \tag{18}$$

where r_T^{new} and z_T^{new} represent the new radial and axial coordinates for the next loop of iteration, $r_T^{present}$ and $z_T^{present}$ represent the coordinates at the end of the present loop, r_T^{old} and z_T^{old} represent the coordinates at the beginning of the present loop, and ω is the relaxation factor. A relaxation factor of 0.5 and 0.35 are used for the calculations of two- and four-bladed rotors, respectively.

The idea of the relaxation is similar to those ideas used in the other relaxation methods, such as the over-relaxation method for solving the elliptic differential equations. First, a unique solution is assumed to exist, then the searching is started by running a proposed initial solution, and the final solution is approached by reducing the errors between successive iterations. In order to apply the relaxation scheme to the tip vortices, each layer of vorticity is separated into two parts, the tip vortex and the inboard vortex sheet. The separation point is the maximum circulation on the blade, since it is assumed that the tip vortex rolls up from the blade tip to the position of maximum circulation. The tip vortex and inboard vortex sheet are stored in different arrays. Whenever the relaxation scheme is applied, the centroid and strength of each tip vortex is calculated by the Simpson rule [8]. The centroids are used as the locations of tip vortices in the relaxation scheme.

Another problem encountered before meaningful results are obtained is the diffusion (or artificial viscosity) problem. This problem originates from the large grid size used in the mesh system. The thickness of the vortex sheet just shed by the

blade is less than 0.5% of the blade radius [8]. According to Rai [10], at least 16 grid points across a Lamb-type vortex core is necessary to prevent excessive numerical diffusion. This is beyond the capability of supercomputers in the near future.

The grid size used in the calculations is 1% of the blade radius (the number of grid points in the r-direction is 161, and is 513 in the z-direction). Each layer of vorticity remains in the computational domain for five to eight blade passages, depending upon the number of vorticity layers used in the iteration process. The vorticity continues to diffuse during the computational process as a result of the strong artificial viscosity. Different layers of vorticity overlap after two to three blade passages. This introduces errors in their interactions and eventually causes the solution to diverge.

To avoid the overlapping, a reconcentration scheme is used. This scheme is applied at the time of blade passage. Each tip vortex is reconcentrated as a Lamb vortex. Its strength is the same as the original tip vortex, and the radius of the core is assumed to be twice the grid size (2% of the blade radius in the present case). Each inboard vortex sheet is divided into subdivisions along the r-direction, typically with every five grid points as the width of a subdivision. The centroid and strength of all the vorticities inside each subdivision are calculated by the Simpson rule [8]. The vorticities inside each subdivision are assumed to be represented by a concentrated Lamb vortex. Its strength equals the sum of the vorticities in the subdivision, its core radius is assumed to be twice the grid size (2% of the blade radius), and its location is the centroid of the vorticities in the subdivision.

A correction to the self-induced velocity of a vortex ring is added to each tip vortex to account for the deficiency caused by the assumption of a large core radius. For a vortex ring, the self-induced velocity is [2]

$$w_o = \frac{\Gamma}{4\pi A}\left[\ln\frac{8A}{a} - \frac{1}{4}\right] \tag{19}$$

where Γ is the strength of the vortex ring, and A and a are its radius and core radius, respectively.

The core radius used in the calculations is 2% of the blade radius. But the tip vortex-core radius of a two-bladed rotor at 60^0 after it is shed by the blade is about 0.3-0.5% of the blade radius [9]. There is a significant difference in the magnitude of the self-induced velocity, especially of the tip vortices. Yet, self-induced velocity is an important mechanism for the descent of tip vortices. A corrective term

$$w_o = \frac{\Gamma}{4\pi A}\left[\ln\frac{8A}{a_{real}} - \ln\frac{8A}{a_{assumed}}\right] \tag{20}$$

is added to each tip vortex at each time step to resolve this deficiency. A value of 0.5% is used for the a_{real}.

Results and Discussions

Encouraging results are obtained after applying the relaxation and reconcentration schemes. The calculations of three different cases has been completed, and the results agree well with experimental data. The first case studied is a Huey 1/7-scale two-bladed rotor [9] with an aspect ratio of 13.7. An uncontracted vortex wake is assumed as the initial shape of the vortex wake. The vorticity contour plot of the initial condition of the Navier-Stokes calculations is shown in Figure 1. A simplified method, which uses a concentrated vortex to represent an inboard vortex sheet, is used for the first four iterations. The position of this concentrated vortex is the centroid of the inboard vortex sheet, and its strength is 80% of the maximum circulation on the blade. The simplified method is chosen because it requires very little computer time; also, its results give a better initial condition for the complex Navier-Stokes calculations. The use of the uncontracted vortex wake as the initial condition is of academic interest but certainly is not practicable.

Figures 2 and 3 show the converging process of the circulation distribution on the blade. Figures 4 and 5 show the converging process of the shape of the vortex wake. From these figures we can see that when an uncontracted vortex wake is first assumed, the peak circulation is relatively flat, since the tip vortex nearest to the blade has a weaker interaction with the blade. This results in a vortex wake which stays closer to the rotor plane.

The peak value of the circulation on the blade seems to be the dominant element in determining the shape of the wake. The tip vortex nearest to the rotor plane has a decisive influence on the thrust coefficient of the rotor. In general, if the tip vortex nearest to the rotor plane stays closer to the rotor plane, it downgrades the thrust coefficient, through inducing downward velocities to the inboard blade. These downward velocities reduce the angles of attack in the inboard portion of the blade and therefore degrade the thrust coefficient. Although the first tip vortex does induce upward velocity to the portion of the blade outboard of it, this outboard portion is small, about 10% of the blade radius (for a standard blade), and cannot compensate the losses in the inboard portion of the blade. The tip vortices immediately below the first one all have a strong tendency to push it upward, since they are located further inboard from the first tip vortex. The far wake pushes the first tip vortex down, but this effect is very limited, about the order of upward induction from the second or the third tip vortex below the first one. The dominant mechanism that pushes the first tip vortex down is its self-induced velocity, which is proportional to the strength of circulation, and in turn is determined by the peak circulation on the blade.

The previous paragraph explains why a small peak circulation results in a denser vortex wake (smaller axial distance between vortex sheets). Curve 2 of Figure 2 shows the effects of this denser vortex wake. There is a high peak circulation, since the tip vortex immediately below the rotor plane stays very close to the plane and induces strong upward velocities to the outboard portion of the blade. But the thrust coefficient actually is lower. Both the shape of the vortex wake and the circulation on the blade converge quite well. This can be seen from the last two curves of Figure 3 and Figure 5, which are almost identical. The numerical thrust coefficient is 0.0086 compared with the experimental value of 0.0087. Figure 6 shows the comparison of the numerical results with the experimental data. The agreement is fairly good considering the uncertainties and difficulties involved numerically and experimentally.

The second case studied is a UTRC's (United Technologies Research Center) linearly twisted two-bladed rotor, which was used by Landgrebe in his hovering-rotor experiment [6]. The twist rate is -6^0 and the aspect ratio is 18.2. Again the circulation on the blade and the shape of the vortex wake converge quite well (Figures 8 through 13). The numerical thrust coefficient is 0.0031 and the test value is 0.0028. The last case studied is an ONERA's (Office National d'Études et de Recherches Aerospatiales) linearly twisted four-bladed rotor [11]. The twist rate is -8.3^0 and the aspect ratio is 15. The relaxation factor used in the relaxation scheme in this case is 0.25, since the solution diverges with a 0.5 relaxation factor. The divergence probably occurs because the spacing between the tip vortices is smaller and therefore is less stable and more sensitive to disturbances. The numerical thrust coefficient is 0.0075 and the test value is 0.0078 (Figures 14 through 19)

In Figures 16 and 17, the tip vortex trajectories move up beyond the rotor plane because of the spline fitting. According to the numerical results, the tip vortex stays very close to the rotor plane for a short time (after it is generated by the passing blade) and then starts moving down; it does not move beyond the rotor plane.

Conclusions

A numerical method based on the Navier-Stokes calculations was developed to predict the vortex wake of hovering rotors. The calculations of three different hovering rotors were completed. When results are compared with hover test data, the agreement is fairly good, considering the difficulties and uncertainties involved numerically and experimentally in the problem. It was found in the Navier-Stokes calculations that a time-marching approach is not adequate for this problem, since the instability grows rapidly during computations. The reason is that the vortex wake of a hovering rotor is extremely unstable, as is confirmed by experiment. The source of instability in the iteration approach is in the tip vortices; there is no instability in the inboard vortex sheets. Some of the instabilities observed in the numerical experiment without applying the relaxation scheme to the tip vortices closely resemble the instabilities observed in hover tests [6][9]. This close resemblance suggests that the tip vortex instability may result from the unstable characteristics of the vortex wake system, not from the numerical scheme. A relaxation scheme is used to diminish the instability during iterations. Another problem encountered is artificial viscosity, which was solved by periodic use of a reconcentration scheme.

References

[1] Liu, C.H., Thomas, J.L., and Tung, C., "Navier-Stokes Calculations for the Vortex Wake of a Rotor in Hover," AIAA Paper 83-1676, July 1983.

[2] Summa, J.M., "Advanced Rotor Analysis Methods for the Aerodynamics of Vortex/Blade Interactions in Hover," Presented at the European Rotorcraft and Powered Lift Aircraft Forum, Sept. 1982.

[3] Lamb, H., "Hydrodynamics," Dover Publications, New York, 1932, p. 241.

[4] Batchelor, G.K., "An Introduction to Fluid Dynamics," pp. 201-206, Cambridge University Press, 1967.

[5] Weston, R.P. and Liu, C.H., "Approximate Boundary Condition Procedure for the Two Dimensional Numerical Solution of Vortex Wakes," AIAA Paper No. 82-0951, 1982.

[6] Landgrebe, A.J., "An Analytical and Experimental Investigation of Helicopter Rotor Hover Performance and Wake Geometry Characteristics," U.S. Army Air Mobility Research and Development Lab. Technical Report 71-24.

[7] Bliss, D.B., Wachspress, D.A., Quakenbush, T.R., and Bilanin, A.J., "A New Approach to the Free Wake Problem for Hovering Rotors," Continuum Dynamics, Inc. Rep. No. 84-7, June 1984.

[8] Gerald, C.F., "Applied Numerical Analysis," Addison-Wesley Publishing Co.,Inc., 2nd edition, 1978.

[9] Tung, C., et al., "The Structure of Trailing Vortices Generated by Model Rotor Blades," NASA TM-81316, Aug. 1981.

[10] Rai, M.M., "Navier-Stokes Simulations of Blade-Vortex Interaction Using High-Order Accurate Upwind Schemes," AIAA Paper 87-0543, Jan. 1987.

[11] Maresca, C., Favier, D., Nsi Mba, M., "A Prescribed Radial Circulation Distribution of a Hovering Rotor Blade," Twelfth European Rotorcraft Forum, Sep. 1986, Garmisch-Partenkirchen, Germany.

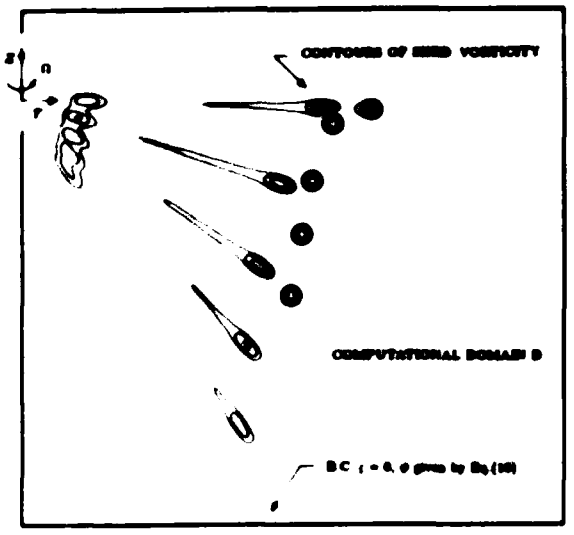

Figure 1 The vorticity contour plot of the initial condition in the Navier-Stokes calculations for the Heavy 1/7-scale two-bladed rotor

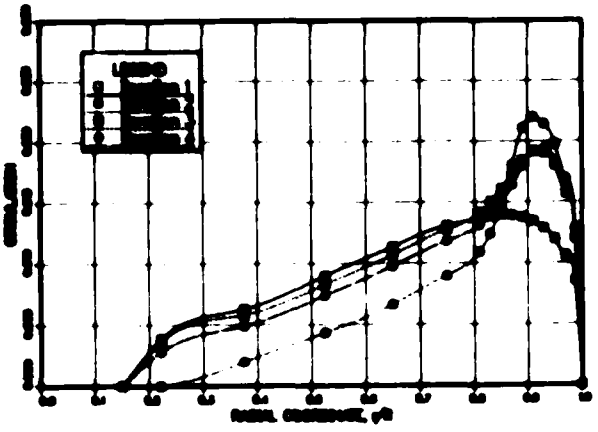

Figure 2 Converging process of the circulation on the blade for the Heavy 1/7-scale two-bladed rotor

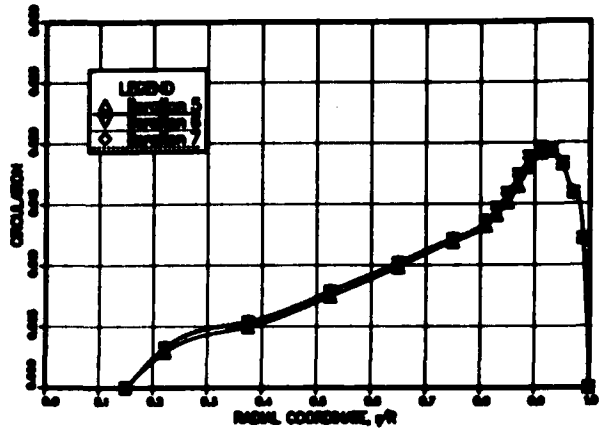

Figure 3: Converging process of the circulation on the blade for the Huey 1/7-scale two-bladed rotor.

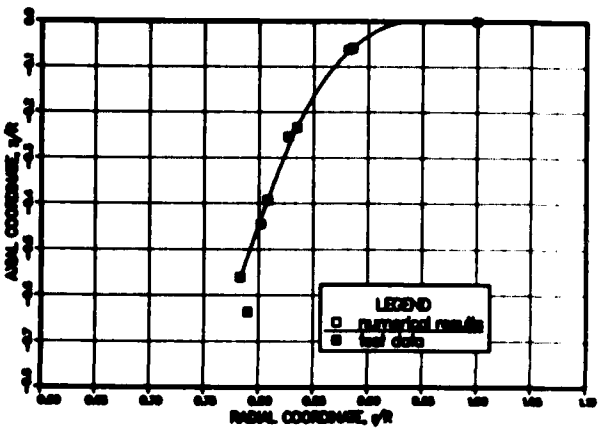

Figure 6: The comparison of numerical results with experimental data for the Huey 1/7-scale two-bladed rotor.

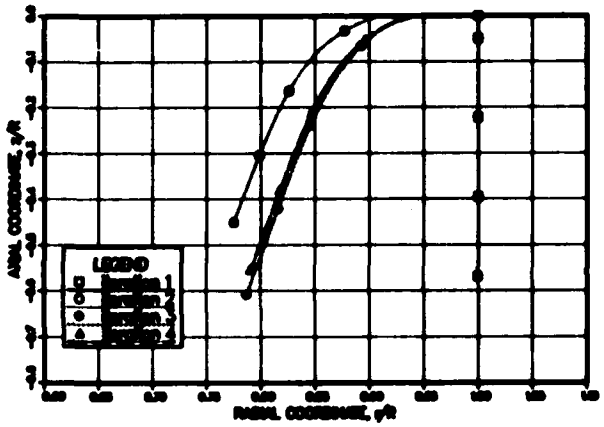

Figure 4: Converging process of the shape of the vortex wake for the Huey 1/7-scale two-bladed rotor.

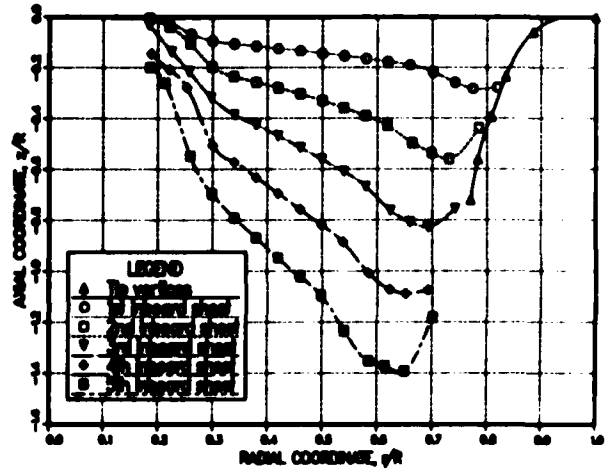

Figure 7: The shape of the converged vortex wake for the Huey 1/7-scale two-bladed rotor.

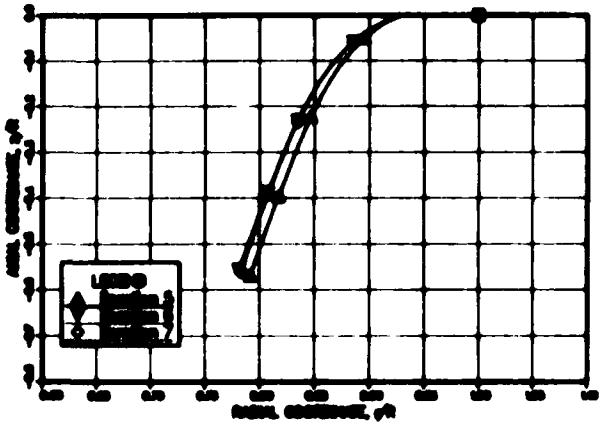

Figure 5: Converging process of the shape of the vortex wake for the Huey 1/7-scale two-bladed rotor.

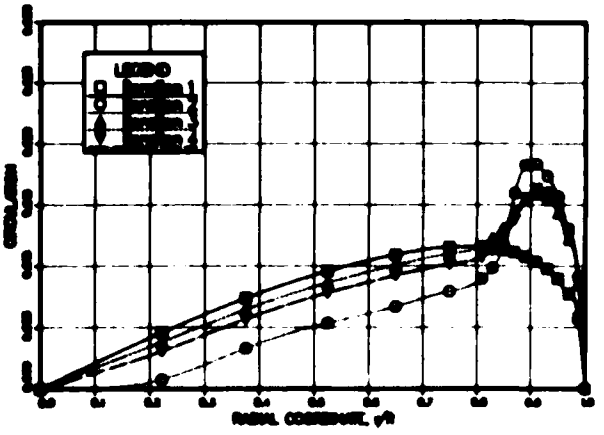

Figure 8: Converging process of the circulation on the blade for UTRC's linearly twisted two-bladed rotor.

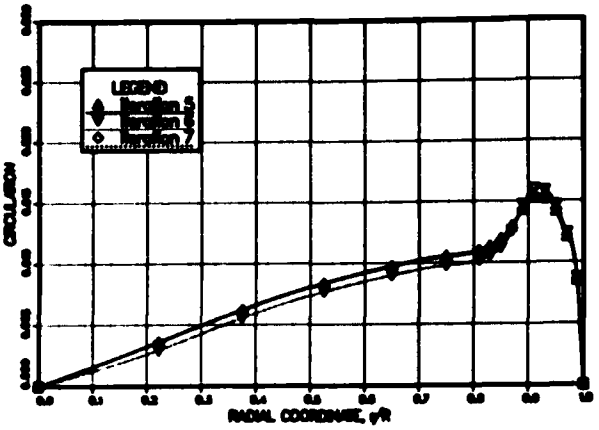

Figure 9: Converging process of the circulation on the blade for UTRC's linearly twisted two-bladed rotor.

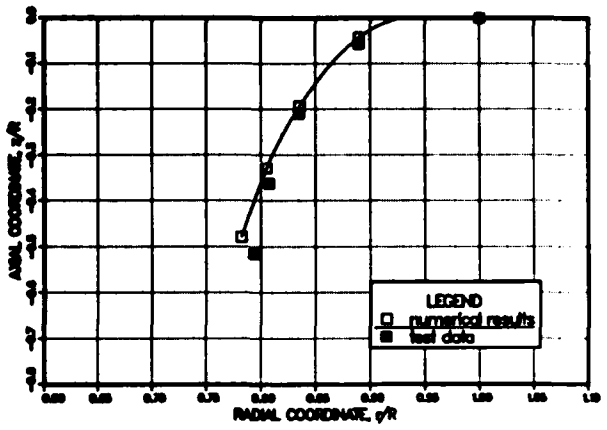

Figure 12: The comparison of numerical results with experimental data for UTRC's linearly twisted two-bladed rotor.

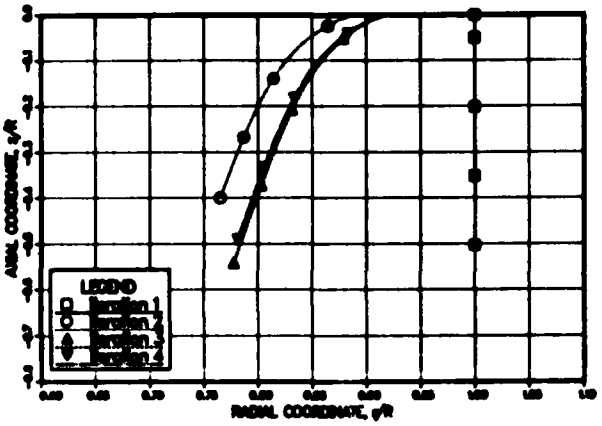

Figure 10: Converging process of the shape of the vortex wake for UTRC's linearly twisted two-bladed rotor.

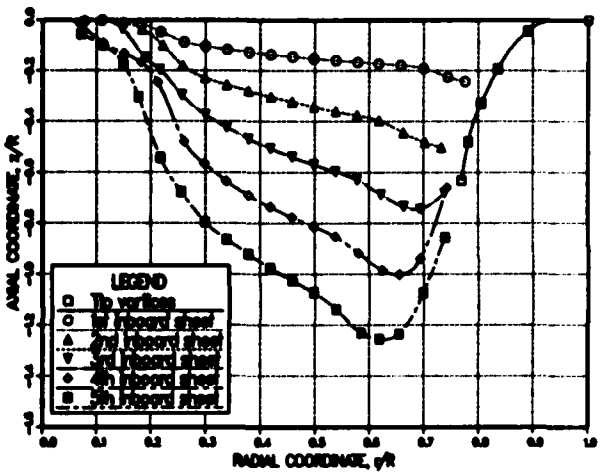

Figure 13: The shape of the converged vortex wake for UTRC's linearly twisted two-bladed rotor.

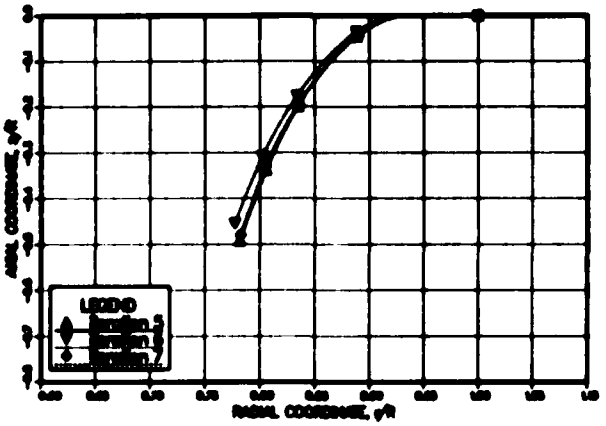

Figure 11: Converging process of the shape of the vortex wake for UTRC's linearly twisted two-bladed rotor.

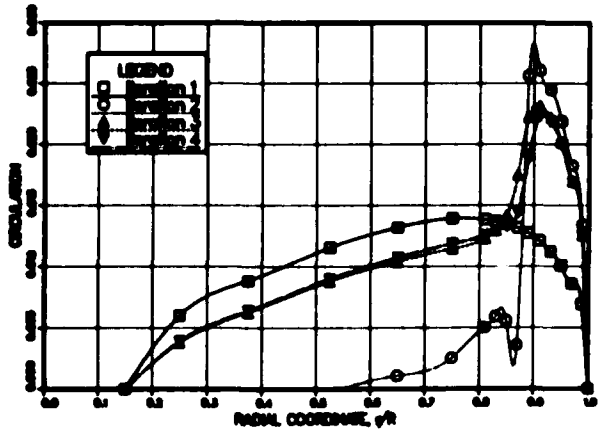

Figure 14: Converging process of the circulation on the blade for ONERA's linearly twisted four-bladed rotor.

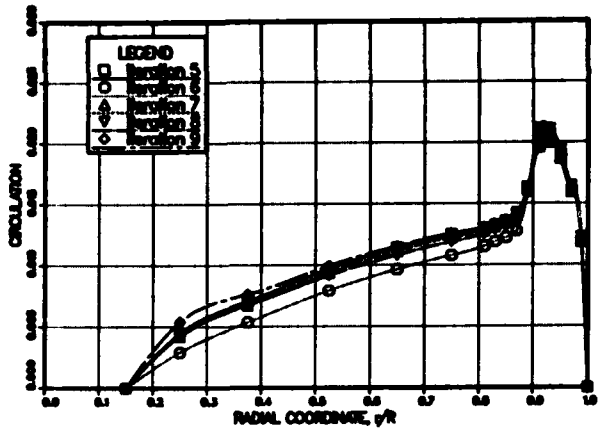

Figure 15: Converging process of the circulation on the blade for ONERA's linearly twisted four-bladed rotor.

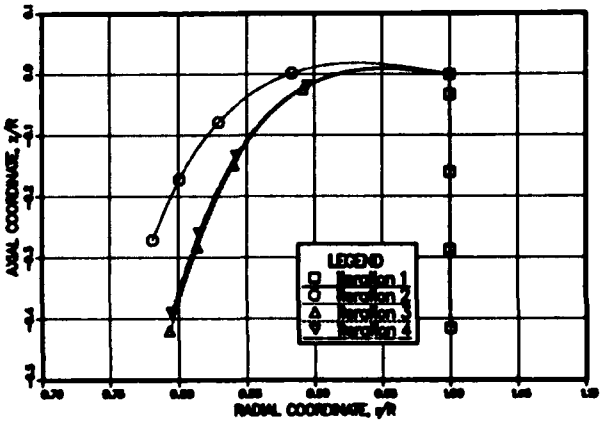

Figure 16: Converging process of the shape of the vortex wake for ONERA's linearly twisted four-bladed rotor.

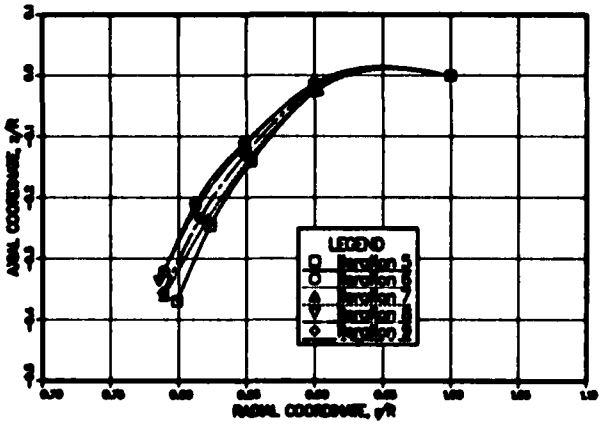

Figure 17: Converging process of the shape of the vortex wake for ONERA's linearly twisted four-bladed rotor.

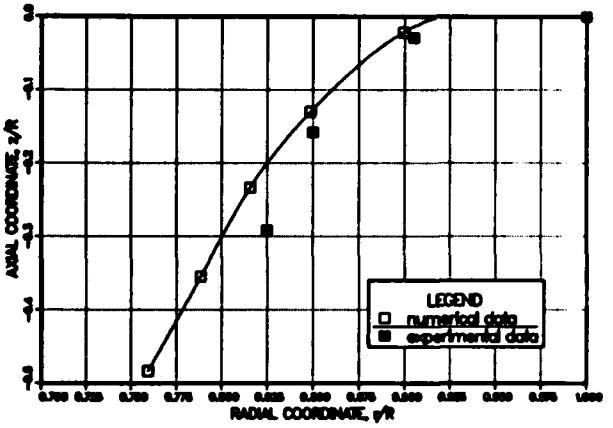

Figure 18: The comparison of numerical results with experimental data for ONERA's linearly twisted four-bladed rotor.

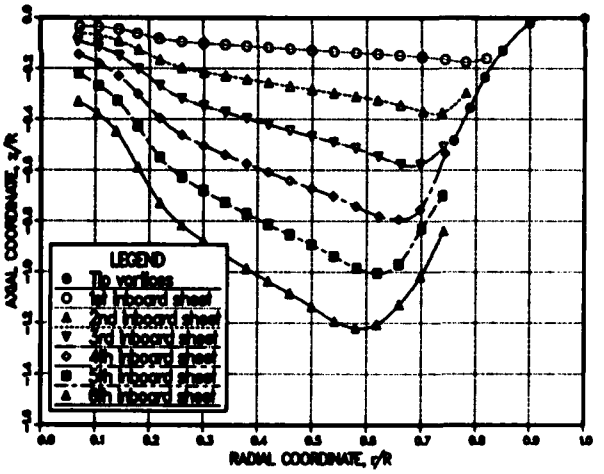

Figure 19: The shape of the converged vortex wake for ONERA's linearly twisted four-bladed rotor.

END

8-87

DTIC